Functional Myoglobin Model Composed of a Strapped Porphyrin/Cyclodextrin Supramolecular Complex with an Overhanging COOH That Increases O(2)/CO Binding Selectivity in Aqueous Solution

Qiyue Mao, Pradip K Das, Stéphane Le Gac, Bernard Boitrel, Vincent Dorcet, Koji Oohora, Takashi Hayashi, Hiroaki Kitagishi

A Functional Myoglobin Model Composed of a Strapped Porphyrin/Cyclodextrin Supramolecular Complex with an Overhanging COOH That Increases O_2/CO Binding Selectivity in Aqueous Solution

Qiyue Mao,[1] Pradip K. Das,[2] Stéphane Le Gac,[2] Bernard Boitrel,[*,2] Vincent Dorcet,[2] Koji Oohora,[3] Takashi Hayashi,[3] and Hiroaki Kitagishi[*,1]

[1]*Department of Molecular Chemistry and Biochemistry, Faculty of Science and Engineering, Doshisha University, Kyotanabe-city, Kyoto 610-0321, Japan*

[2]*Univ Rennes, CNRS, ISCR (Institut des Sciences Chimiques de Rennes), UMR 6226, Rennes, F-35000, France*

[3]*Department of Applied Chemistry, Graduate School of Engineering, Osaka University, 2-1 Yamadaoka, Suita 565-0871, Japan*

*Correspondence to: bernard.boitrel@univ-rennes1.fr, hkitagis@mail.doshisha.ac.jp

Abstract: A water-soluble strapped iron(III)tetraarylporphyrin (**Fe^{III}Por-1**) bearing two propyl pyridinium groups at the side chains and a carboxylic acid group at the overhanging position of the strap was synthesized to mimic the function of myoglobin with the distal polar functionality in aqueous solution. **Fe^{III}Por-1** forms a stable 1:1 inclusion complex with a per-*O*-methylated β-cyclodextrin dimer having a pyridine linker (**Py3OCD**), providing a hydrophobic environment and a proximal fifth ligand to stabilize the O_2-complex. The ferrous complex (**Fe^{II}PorCD-1**) binds both O_2 and CO in aqueous solution. The O_2 and CO binding affinities ($P_{1/2}^{O2}$ and $P_{1/2}^{CO}$) and half-life time ($t_{1/2}$) of the O_2 complex of **Fe^{II}PorCD-1** are 6.3 and 0.021 Torr, and 7 h, respectively, at pH 7 and 25°C. The control compound without the strap structure (**Fe^{II}PorCD-2**) has similar oxygen binding characteristics ($P_{1/2}^{O2}$ = 8.0 Torr), but much higher CO binding affinity ($P_{1/2}^{CO}$ = 3.8 x 10^{-4} Torr), and longer $t_{1/2}$ (30 h). The O_2 and CO kinetics indicate that the strapped structure

in **Fe^{II}PorCD-1** inhibits the entrance of these gaseous ligands into the iron(II) center, as evidenced by lower k_{on}^{O2} and k_{on}^{CO} values. Interestingly, the CO complex of **Fe^{II}PorCD-1** is significantly destabilized (relatively larger k_{off}^{CO}), while the k_{off}^{O2} value is much smaller than that of **Fe^{II}PorCD-2**, resulting in significantly increased O_2/CO selectivity (reduced *M* value, where $M = P_{1/2}^{O2}/P_{1/2}^{CO} = 320$) in **Fe^{II}PorCD-1** compared to **Fe^{II}PorCD-2** ($M = 21000$).

Introduction

Myoglobin (Mb) and hemoglobin (Hb) are responsible for storage and transportation of molecular oxygen (O_2) in mammals.[1,2] Researchers have been investigating how these proteins discriminate carbon monoxide (CO) from O_2 because CO is a potential competing gaseous ligand for these proteins.[3–5] In both Mb and Hb, heme is bound by a proximal histidine (His) and surrounded by polar amino acid residues including a distal His (Figure 1a). The axial coordination from the proximal His is essential to form a stable iron–O_2 (CO) coordination bond through π-back donation. Biochemical studies using Mb mutants have revealed that His64 at the distal site plays an essential role in stabilizing the Fe^{II}–O_2 complex through a hydrogen bonding interaction.[3] Distal His64 also plays a role in decreasing the binding of CO to heme. As the original affinity of the heme prosthetic group (alone) for CO is about 2×10^4 higher than that for O_2, the two concomitant effects (hydrogen bond stabilization of O_2 / steric constraint destabilization of CO) derived from the distal histidine in native hemoproteins allows to decrease the ratio of the CO affinity versus the O_2 affinity around 30. This ratio, described as the partition coefficient or $M = K_{CO}/K_{O2} = P_{1/2}^{O2}/P_{1/2}^{CO}$, represents the O_2/CO selectivity or discrimination and is probably the most difficult property to reproduce in heme model systems. Therefore, in the last few decades of biomimetic model studies, introducing a distal functionality into synthetic iron(II)porphyrins to improve the O_2/CO selectivity, that is, reducing the affinity of CO with respect to that of O_2 was an eternal challange.[4,5] The very first synthetic Mb model, recognized as Collman's picket-fence porphyrin (Figure 1b), demonstrated high CO binding affinity and low O_2/CO selectivity (a relatively large *M* value) compared to native Mb because of the lack of distal functionality. Other synthetic models which include distal capped structure were found to demonstrate significantly reduced *M* values (Figure 1c and d) due to both steric and polar repulsion of CO coordinated to the iron(II)porphyrins. The polar repulsion has proven very effective as well to reduce the CO binding affinity, as demonstrated by the model compounds synthesized by Naruta et al.

(Figure 1e).[6,7]

As shown in Figure 1b-e, most of the synthetic Mb models function in organic solvents. The process of binding of O_2/CO to these compounds have been mostly characterized in anhydrous organic solvents such as absolute toluene. In native Mb and Hb, heme is encapsulated in the heme pocket, preventing an irreversible water-catalyzed autoxidation reaction[8,9] that is difficult to avoid in model systems. Using per-*O*-methylated β-cyclodextrin (**TMe-β-CD**) as a heme pocket alternative, tetraarylporphyrins and their iron complexes can be isolated into the hydrophobic environment in aqueous media.[10–12] The most advanced system to mimic the O_2/CO binding function of Mb in aqueous solution is the supramolecular system, **hemoCD**, composed of 5,10-15,20-tetrakis(4-sulfonatophenyl)porphinatoiron(II) (**Fe^{II}TPPS**) and the **TMe-β-CD** dimer, where the proximal axial ligand is mimicked by the nitrogenous linker of the dimer (Figure 1f).[13–15] To the best of our knowledge, **hemoCD** and its related compounds are the only well-established biomimetic models of Mb that bind O_2 and CO reversibly in aqueous solution at room temperature. Therefore, introduction of the distal functionality into **hemoCD** holds promise to provide a more sophisticated Mb model that functions in aqueous solution.

Several different types of CD dimers have been synthesized as water-soluble biomimetic Mb/Hb models.[15] Among these models, the CD dimer **Py3OCD** is the leading compound of apo-myoglobin-mimic, whose inclusion complex with **Fe^{II}TPPS** (**hemoCD3**, Figure 1f) forms the most stable O_2–adduct with the longest half-life time among the **hemoCD** derivatives (50 h at pH 7 and 25^{o}C).[16,17] In the present study, distal functionality has been introduced to the **hemoCD3** scaffold, and its O_2 and CO binding properties have been characterized in thermodynamic and kinetic experiments. In order to introduce the distal functionality into **hemoCD3**, we have adopted the strapped porphyrin system. Introduction of the strapped structure into a metalloporphyrin expands its molecular design from 2D to 3D, providing a powerful strategy to develop new porphyrin-based functional materials[18–20] including biomimetic models with distal functionality.[4,21–23] Among the strapped porphyrins, we selected an overhanging carboxylic acid structure because our previous synthetic model study (Figure 2) demonstrated enhanced O_2 binding affinity with reduced CO binding affinity, resulting in improved *M* value in organic solvent.[23–25] Here, we have newly synthesized an iron complex of water-soluble strapped porphyrin bearing both an overhanging carboxylic acid and two pyridinium groups (**Fe^{II}Por-1**, Figure 3). The effect of distal COOH on binding of O_2 and CO to **Fe^{II}Por-1** encapsulated into the molecular container **Py3OCD** is investigated in aqueous solution.

Results and Discussion

Synthesis of the strapped porphyrin (Fe^{III}Por-1)

The iron complex of strapped porphyrin **Fe^{III}Por-1** equipped with an overhanging COOH and two pyridinium groups, was synthesized according to Scheme 1. Porphyrin **2** was prepared according to a previously reported procedure.[26] Decarboxylation of **2** by heating in DMF at 115 °C afforded **3**, whose inner nitrogen atoms and carboxylic acid group were protected by metalation with $Bi(NO_3)_3$ to give **3Bi**. Reaction of **3Bi** with dibromopropane in DMF gave the bis-bromo-alkylated compound **4**. Finally, **4** was heated in pyridine for 8h and converted to the water-soluble bis-bromopyridinium complex **1Bi**. The removal of bismuth ion was achieved by treatment of **1Bi** by hydrobromic acid, delivering free-base porphyrin **1,** which was metalated by $FeBr_2$ in the presence of 2,6-lutidine to obtain **Fe^{III}Por-1** after exposure to air. The structure of **Fe^{III}Por-1** (Scheme 1) is represented with a carboxylate-bound ferric cation by analogy with the X-ray structure of the bis-hydroxy analogous complex.[27]

The structure of porphyrin **3** was resolved by solid state by X-ray crystallography (Figure 4, top) and confirmed the presence of only one carboxylic group on the strap. The macrocycle is significantly saddle-shaped as indicated by the average off-plane location of the two sets of four opposite β-pyrrolic carbon atoms (+0.485 Å and -0.459 Å). The strap does not exhibit any particular conformation but is slightly twisted with the overhanging carboxylic group disordered over two positions. In its closest position represented in Figure 4, the hydroxyl oxygen atom O1 of the carbonyl functional group is located 2.823 Å away from the N4-centroid of the porphyrin but 7.746 Å away in the other disordered position. These two possible positions indicate that the strap, although pre-organized, remains flexible and mobile without any coordination driving force.

The X-ray structure of **3Bi** was solved as well (Figure 4, bottom). At the opposite of the free-base porphyrin **3**, the strap in the bismuth complex is clearly frozen in a "W-shape" conformation. This specific conformation allows the overhanging carboxylic group to be oriented towards the cavity and to bind the bismuth cation (O1-Bi = 2.549 Å) as found in most of the metal complexes obtained from this type of strap porphyrin.[28] The latter, bound 1.224 Å away from the 24-atom mean plane, induces a domed-shape of the porphyrin with Bi-N bond lengths ranging from 2.286 to 2.399 Å. It should be noted that the X-ray structure of **3Fe** has been previously reported and demonstrates that, although iron is coordinated only 0.449 Å away from the 24-atom mean plane of the macrocycle, the

intramolecular carboxylate can still coordinate the ferric cation (O1-Fe 1.997 Å).[27]

O_2 and CO coordination to Fe^{II}PorCD-1

Fe^{III}Por-1 is soluble in water and has typical Soret and Q-bands at 418 and 575 nm, respectively (Figure 5a). Addition of **Py3OCD** to the solution causes a spectral change with new Soret and Q-bands at 422 and 527 nm, respectively, due to the porphyrin complexation. A titration experiment (Figure 5b) indicates a gradual spectral change with several isosbestic points. The titration curve (Figure 5b inset) indicates a 1:1 stoichiometric complexation between **Fe^{III}Por-1** and **Py3OCD**, with a binding constant estimated as $K = 1.4 \times 10^6$ M^{-1}. Electrospray mass spectrometry (ESI-MS) measurements of the mixture of **Fe^{III}Por-1** and **Py3OCD** in water (Figure 5c) indicates the presence of a 1:1 complex between them, whose isotope pattern corresponds to the theoretical complex (Figure 5c inset).

The **Fe^{III}PorCD-1** complex was reduced to its ferrous form (**Fe^{II}PorCD-1**) with addition of excess sodium dithionite ($Na_2S_2O_4$). The ferrous complex has its Soret and Q-bands at 435 and 529 nm, respectively (Figure 6, green line), which is attributed to **Fe^{II}PorCD-1** in the deoxy form, where excess dithionite consumes O_2 in water. It is notable that the λ_{max} values are essentially identical to those observed in **hemoCD3** (434 and 530 nm), indicating that the overhanging COOH in **Fe^{II}PorCD-1** does not coordinate to the iron(II) center. As an additional evidence, the distal overhanging COOH of the analogous bis-strapped ferrous porphyrin bearing a built-in proximal nitrogen base (αβ-OCAFe, Figure 2) is unable to coordinate the iron center and the complex remains five-coordinate as shown by both its paramagnetic proton NMR spectrum typical of a high spin ($S = 2$) complex and UV-vis spectrum with the Soret band at 439 nm.[20] After reduction, excess $Na_2S_2O_4$ and its oxidized byproduct were removed by passing the sample through a Sephadex G-25 column conducted under aerobic conditions. The gel filtration process was completed within 5 min. The UV-vis spectrum of the resulting eluted solution exhibiting Soret and Q-bands at 422 and 543 nm, respectively (Figure 6, red line), was attributed to the O_2-adduct, **O_2-Fe^{II}PorCD-1**. To the solution of **O_2-Fe^{II}PorCD-1**, CO gas was then introduced for 20 sec, to induce the expected changes in the spectrum, especially the sharper Soret band (Figure 6, blue line). As CO is known not to coordinate to Fe^{III}-porphyrins, this spectral change indicates that in the eluted complex **O_2-Fe^{II}PorCD-1**, the iron is formally still in its ferrous form, otherwise no ligand exchange would be observed. Therefore, **Fe^{II}PorCD-1** does act as a dioxygen carrier that can first bind dioxygen and then release it. Although no direct spectroscopic

investigation has been performed about the electronic structure of the oxy-adduct, it is reasonable to describe it as the resonance limit equation, Fe^{II}-O_2 ↔ Fe^{III}-$O_2^{\bullet}$.

The **O_2-Fe^{II}PorCD-1** complex was gradually autoxidized to the ferric met-form (**Fe^{III}PorCD-1**) (Figure S1 in Supporting Information). The first-order rate constant (k_{obs}) for the autoxidation reaction is 0.1 h^{-1} ($t_{1/2}$ = 7.0 h) in aqueous solution at pH 7.0 and 25°C. Compared to **hemoCD3** without the strap structure (Figure 1f), whose O_2-adduct shows a $t_{1/2}$ = 50 h under the same conditions, the autoxidation of **O_2-Fe^{II}PorCD-1** was significantly faster. This is likely because water molecule(s) can more easily gain access to the iron(II) center as a result of the cleft of the CD dimer in the **O_2-Fe^{II}PorCD-1** complex being sterically widened by its strap structure.

CO and O_2 binding affinities of Fe^{II}PorCD-1 and its related compounds

The CO and O_2 binding affinities and the selectivity (*M* value) of **Fe^{II}PorCD-1** were measured in aqueous buffer solution at pH 7.0 and 25°C. The CO binding affinity was first measured based on the spectral change of **Fe^{II}PorCD-1** as a function of the CO partial pressure (P^{CO}) in N_2 in the presence of excess sodium dithionite (Figure 7a). The spectral changes indicated transformation from **Fe^{II}PorCD-1** to **CO-Fe^{II}PorCD-1** with clear isosbestic points. The curve fitting analysis provided the CO binding affinity as $P_{1/2}^{CO}$ value, defined by the following equation.[14,21]

$$P_{1/2}^{CO} = [\mathbf{Fe^{II}PorCD\text{-}1}]\, P^{CO}/[\mathbf{CO\text{-}Fe^{II}PorCD\text{-}1}] \quad (1)$$

From the titration experiment, $P_{1/2}^{CO}$ was determined to be (2.1 ± 0.8) × 10^{-2} Torr (average ± SD in 3 independent experiments). This $P_{1/2}^{CO}$ value is significantly larger than that of **hemoCD3** (5.6 × 10^{-4} Torr), indicating much lower (two orders of magnitude) CO binding affinity for **Fe^{II}PorCD-1**. To determine O_2/CO selectivity, the CO titration experiment was performed under an O_2 atmosphere without dithionite (Figure 7b). The spectral changes indicate transformation from **O_2-Fe^{II}PorCD-1** to **CO-Fe^{II}PorCD-1** with clear isosbestic points. The O_2/CO selectivity, quantified by the *M* value, defined in eq (2), was determined based on the O_2 and CO partial pressures, P^{O2} and P^{CO}, with equal concentrations of **O_2-** and **CO-Fe^{II}PorCD-1** in solution.[4,14,29]

$$M = P_{1/2}^{O2}/\, P_{1/2}^{CO} = \{[\mathbf{CO\text{-}Fe^{II}PorCD\text{-}1}]\, P^{O2}\}/\{[\mathbf{O_2\text{-}Fe^{II}PorCD\text{-}1}]\, P^{CO}\} \quad (2)$$

The M value of **Fe^{II}PorCD-1** was determined to be 320 ± 52 (average ± SD in 3 independent experiments) based on the curve fitting analysis of the titration curve (for analysis details, see the Experimental section). The M value was significantly smaller than that of **hemoCD3** (3.2×10^4), suggesting that the overhanging COOH group functions as a distal polar group as in native Hb/Mb. Here we assume that the COOH group in **Fe^{II}PorCD-1** exists as the non-dissociated form on the basis of the C–O stretching data for **CO-Fe^{II}PorCD-1** as discussed below. The O_2 binding affinity, defined as $P_{1/2}{}^{O2}$ (eq 3), was determined from the $P_{1/2}{}^{CO}$ and M values.[4,14,29]

$$P_{1/2}{}^{O2} = [\textbf{Fe}^{II}\textbf{PorCD-1}]\, P^{O2}/[\textbf{O}_2\textbf{-Fe}^{II}\textbf{PorCD-1}] \quad (3)$$

To clearly understand the effect of the overhanging COOH in **Fe^{II}PorCD-1** on the O_2/CO bindings, **Fe^{II}PorCD-2** having the same alkyl pyridinium substitutes as **FePorCD-1** was prepared using the iron(II) complex of **TPPOC3Py** (**Fe^{II}Por-2**)[11] and **Py3OCD**. The **Fe^{II}PorCD-2** complex forms its O_2 and CO complexes similar to **Fe^{II}PorCD-1** in aqueous buffer solution at 25°C (Figure S2 in Supporting Information). The $t_{1/2}$ for the autoxidation of **O$_2$-Fe^{II}PorCD-2** is 30 h, which is considerably longer than that of **O$_2$-Fe^{II}PorCD-1** ($t_{1/2}$ = 7 h) under the same experimental conditions. This supports the assumption that the sterically wider cleft of the CD dimer in the strapped **O$_2$-Fe^{II}PorCD-1** complex accelerates the autoxidation process in aqueous solution. The relationship between the steric factor of the cleft and the water-promoted autoxidation rates of the oxy-complexes has been discussed elsewhere.[14,15] The CO and O_2 binding affinities and M value were determined as described for **Fe^{II}PorCD-1**. These thermodynamic parameters for CO and O_2 binding are summarized in Table 1.

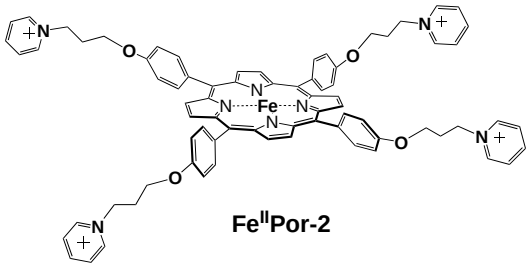

Fe^{II}Por-2

Among the series of porphyrin/cyclodextrin supramolecular systems, **Fe^{II}PorCD-1** shows a significantly small M value (320), which is similar to that of native Hb in the R state (150) and the **TCP-PY** system which has a proximal pyridine and a distal OH group (550). The $P_{1/2}{}^{O2}$ and $P_{1/2}{}^{CO}$

values of **Fe^{II}PorCD-2** are approximately half of the values of **hemoCD3**. This is likely due to the different porphyrin substituents (pyridinium vs sulfonatophenyl groups). When these values are compared between **Fe^{II}PorCD-1** and **Fe^{II}PorCD-2**, the CO affinity of **Fe^{II}PorCD-1** is *ca.* 100-times lower than that of **Fe^{II}PorCD-2** with no significant difference in the O_2 affinities. The CO binding affinity and *M* value of **hemoCD3** are very similar to those of **Fe^{II}PorCD-2**, which does not have a strap structure. Therefore, introduction of the strap structure with an overhanging COOH causes a significant effect on the process of binding of CO to the iron(II)porphyrin. A plausible mechanism is discussed in the following section based on the kinetic data.

Kinetic study of the CO and O_2 binding

The rate constants for O_2 and CO binding were measured by laser flash photolysis.[14] The absorbance at 435 nm, which is λ_{max} of **Fe^{II}PorCD-1** in the deoxy-form (see Figure 6), temporarily increases followed by regeneration upon laser flash irradiation (532 nm) to the **CO-Fe^{II}PorCD-1** solution due to its photo-dissociation and rebinding processes (Figure 8a). Kinetic studies of **Fe^{II}PorCD-2** and **hemoCD3** were also conducted. Compared to the kinetic profile of **CO-Fe^{II}PorCD-2** (Figure 8a, blue line), the CO rebinding process is clearly slow for **CO-Fe^{II}PorCD-1** (Figure 8a, red line). The CO rebinding process to **Fe^{II}PorCD-1** is obviously inhibited due to its strapped structure. The single-exponential curve fitting analysis for the absorbance decay yields the observed rate constants for the rebound processes of CO to the porphyrin (k_{obs}^{CO}). Consistently, absorbance decay (dissociation) followed by an increase in intensity (recombination) were observed at 422 nm and ascribed to λ_{max} of **CO-Fe^{II}PorCD-1** (Figure S3 in Supporting Information). The second-order rate constants (k_{on}^{CO}) were determined based on the linear regression of the k_{obs}^{CO} values as a function of [CO] in the solution (Figure 8b) (eq 4).[5–7,14,30,31]

$$k_{obs}^{L} = k_{on}^{L}\,[L] + k_{off}^{L}\ (L = CO \text{ or } O_2) \qquad (4)$$

The binding kinetics for O_2 were also examined using the respective O_2 complexes of **hemoCD3**, **Fe^{II}PorCD-1** and **Fe^{II}PorCD-2**, with the same laser apparatus (Figure S4 in Supporting Information). Table 2 shows the kinetic data generated in the present study with reference data. Interestingly, both the k_{on}^{O2} and k_{on}^{CO} values of **Fe^{II}PorCD-1** are significantly smaller than those of **hemoCD3** and **Fe^{II}PorCD-2**, suggesting that the strap structure of **Fe^{II}PorCD-1** sterically inhibits the entrance of

these gaseous ligands into iron(II) active site. As discussed above, the intramolecular coordination of the overhanging carboxylic group on the ferrous cation has been ruled out. In the 5,15-conformation of the strap, this type of coordination is only possible with cations significantly bound out-of-plane (OOP) of the porphyrin towards the distal side. This is the case either for bismuth(III) (Figure 4, OOP = 1.224 Å) or iron(III) (OOP = 0.449 Å).[27] Similar steric inhibition was found in the model studies (*e.g.*, **Picket-fence Por** versus **FePocPiv,** see Table 2). On the other hand, the release of CO (k_{off}^{CO}) from **CO-Fe^{II}PorCD-1** is much faster, resulting in lower CO binding affinity for **Fe^{II}PorCD-1** than for **hemoCD3** and **Fe^{II}PorCD-2**. Concerning k_{off}^{O2}, the release of O_2 from **O$_2$-Fe^{II}PorCD-1** is significantly suppressed compared to **hemoCD3** and **Fe^{II}PorCD-2**. This is likely due to the overhanging COOH strap structure. From the kinetic data, it was determined that the polar distal functionality of **Fe^{II}PorCD-1** causes destabilization of the CO-complex (relatively large k_{off}^{CO}) while stabilizing the O_2-complex (relatively small k_{off}^{O2}). This results in improvement of the *M* value (320), which is somewhat close to that of native Mb/Hb. A plausible mechanism for this phenomenon is discussed in the next section in context of vibrational spectroscopic data.

The effect of the overhanging COOH on the O$_2$- and CO-complexes

To investigate how the overhanging carboxylic acid of **Fe^{II}PorCD-1** affects the dynamics of the gaseous ligand bound to the iron(II) center, the C–O bond stretching frequency (ν_{CO}) of **CO-Fe^{II}PorCD-1** was measured by infrared (IR) spectroscopy and compared to spectra of the CO-complexes without the strap structure. Figure 9 shows the IR spectra of **CO-Fe^{II}PorCD-1**, **CO-Fe^{II}PorCD-2**, and **CO-hemoCD3** in aqueous buffer solution at room temperature. In these spectra, ν_{CO} bands were detected at 1971, 1981, and 1985 cm^{-1}, respectively. Therefore, the overhanging carboxylic acid causes approximately a 10 cm^{-1} lower shift in ν_{CO} of the CO-complex. Compared to native Mb and its distal mutant (H64G), whose ν_{CO} values are 1947 and 1965 cm^{-1},[32] the overhanging carboxylic acid in **Fe^{II}PorCD-1** functions as a distal polar functional group in a manner similar to His64 in native Mb. The 10 cm^{-1} lower shift in ν_{CO} of the **CO-Fe^{II}PorCD-1** complex indicates decrease of the C–O bond order. When proton donor(s) such as His64 in Mb/Hb exists around the distal site, the C–O bond order of the Fe–CO complex decreases because of the formation of $Fe^{\delta+}=C=O^{\delta-}\cdots H^{\delta+}$ resonance structure (*i.e.*, the positive polar effect).[33,34] Therefore, the observed ν_{CO} change in the strapped porphyrin suggests the existence of intramolecular interaction between Fe–CO and distal COOH.

Olson et al. reported a linear correlation between k_{off}^{CO} and ν_{CO} in Mb mutants; a higher ν_{CO} wavenumber is related to faster dissociation of CO from heme due to weakening the π-back-bonding from Fe to CO.[32] It is notable that this trend is not observed in the present system; **CO-Fe^{II}PorCD-1** has a lower ν_{CO} and a higher k_{off}^{CO} compared to **CO-hemoCD3** and **CO-Fe^{II}PorCD-2**. Therefore, the accelerated dissociation of CO from **CO-Fe^{II}PorCD-1** is not ascribed to weak π-back bonding from Fe to CO but to the repulsion due to the distal COOH group in **Fe^{II}PorCD-1**. We previously showed that high CO binding affinity of **hemoCD1** ($P_{1/2}^{CO}$ = 1.5 × 10^{-5} Torr), a synthetic analogue of **hemoCD3** composed of **Fe^{II}TPPS** and a CD dimer with a pyridine linker, is ascribed to very slow off rate (k_{off}^{CO} = 2.5 × 10^{-4} s^{-1}) regardless of weak π-back-bonding from Fe to CO.[14] The off rate constant of **hemoCD1** is the lowest among the heme proteins and model complexes reported so far.[35] Capturing CO in the hydrophobic cleft of **hemoCD1** causes slow dissociation due to the lipophilic nature of CO.[36] In the optimized molecular structure of **CO-Fe^{II}PorCD-1** shown in Figure 10, the overhanging COOH group of **CO-Fe^{II}PorCD-1** is oriented towards the axial CO ligand due to its pre-organized "W-shape" structure, as evidenced by crystal structure of the precursors (see Figure 4). Insertion of a polar COOH functional group into the cleft of the CD dimer causes repulsion with CO in **CO-Fe^{II}PorCD-1**, accelerating dissociation of CO from the cleft to aqueous bulk phase.

While the CO-complex of **Fe^{II}PorCD-1** is significantly destabilized by the overhanging COOH, the O_2-adduct of **Fe^{II}PorCD-1** has a much lower k_{off}^{O2} value (Table 2). Consequently, **Fe^{II}PorCD-1** has moderate O_2 binding affinity (6.3 Torr) comparable to that of **Fe^{II}PorCD-2** (8.0 Torr) which does not have a strap. This is consistent with the tendency observed in the synthetic models in organic solvent; the stabilization effect has been observed in the O_2 complexes of iron(II) or cobalt(II) porphyrins bearing an overhanging COOH.[25,37] These models demonstrated that the overhanging COOH functions efficiently as a hydrogen atom donor similar to the distal His64 in native Mb. In the present system in aqueous solution, the overhanging COOH may also function as a distal H-donor in stabilizing the O_2 complex. The overhanging COOH group enters the ligand-binding site (Fe^{II} center) at the hydrophobic cleft of the CD dimer (Figure 10); thus, it can directly interact with coordinated O_2 or CO. As discussed above, the lower shift of ν_{CO} observed in **CO-Fe^{II}PorCD-1** suggests the existence of an electrostatic interaction between the oxygen atom of **Fe^{II}–CO** and the vicinity of the H-donor,[38–40] supporting our proposal that the overhanging COOH exists as the non-dissociated form. In the pH titration experiments for the **Fe^{III}PorCD-1** complex in water, no characteristic spectral change at the pH region from 4 to 10 were detected, suggesting that the distal

COOH has lower acidity than normal carboxylic acid groups in aqueous solution.[41] The hydrophobic environment created by the CD cavity can isolate the COOH group from the aqueous bulk phase, suppressing the acid-dissociation of COOH even at the neutral pH, as observed in aqueous-organic solvents[42] or in the isolated hydrophobic pockets in water.[43,44]

Conclusion

The present study demonstrates the functionality of a water-soluble Mb functional model which includes both a proximal ligand and a distal polar environment. The hydrophobic heme pocket and the proximal ligand are constructed with a cyclodextrin dimer which includes a pyridine linker (**Py3OCD**). The distal polar environment includes the strap structure of a porphinatoiron(II) complex bearing an overhanging carboxylic acid (**FePor-1**). As expected, the 1:1 supramolecular complex **Fe^{II}PorCD-1** functions as a water-soluble Mb functional model with both a proximal ligand to iron(II) and distal polar functionality. It is remarkable that the distal COOH group directed to the iron(II) center located at the hydrophobic cavity of the CD dimer causes a "kick off" effect with respect to coordinated CO, while it has the opposing influence, in stabilization of coordinated O_2. Therefore, the distal overhanging COOH group in the present model system shows the best O_2/CO selectivity among the aqueous Mb biomimetics reported so far. We believe that the combination of strapped porphyrins and cyclodextrin dimer systems can expand existing molecular design strategies by reproducing both the proximal and distal functionalities of native heme proteins such as catalase, cytochrome P450, and cytochrome *c* oxidase in aqueous solution.

Experimental Section

Materials. Py3OCD, **Fe^{III}TPPS**, and **FePor-2** were synthesized as previously reported.[11,12,16] Other reagents and solvents were purchased and used as received. Pure O_2 (99.999%), pure N_2 (99.999%), and diluted CO (0.0909% in N_2) gases were purchased from Sumitomo Seika Chemicals. For flash photolysis, pure CO (99.95%) from Sumitomo Seika Chemicals was used.

Instruments. Electrospray ionization time-of-flight (ESI-TOF) mass spectra were taken on a JEOL JMS-T100CS spectrometer. UV-vis spectra were measured using a Shimadzu UV-2100 and UV-2450 spectrophotometer (Kyoto, Japan). Kinetic measurements were performed using a laser flash photolysis system manufactured by Unisoku (Osaka, Japan) with a 5 ns pulse laser beam from a Q-

switched Nd:YAG laser (Surelite I, Continuum). Mixed O_2 gases with various partial pressures in N_2 and mixed CO gases with various partial pressures in O_2 were prepared with a KOFLOC GM-4B gas mixing apparatus (Kyoto, Japan). IR spectra were measured using a Shimadzu IR Prestige-21.
For the synthesis of **Fe^{III}Por-1**, electrospray ionization high resolution mass spectra (ESI-HRMS) were recorded on a Micromass MS/ MS ZABSpec TOFF spectrometer and MALDI-TOF spectra on a Microflex-LT Bruker Daltonics (C.R.M.P.O. University of Rennes 1). ^{1}H- and ^{13}C-NMR spectra were recorded on a BrukerAvance500 spectrometer equipped with a BBFO probe. Spectra were referenced with residual solvent protons. For detailed labeling of protons, see supplementary information, pages S16-S17. UV-vis spectra were recorded on an Uvikon XL spectrometer. THF (K/benzophenone, N_2) was distilled before use.

Synthesis of Fe^{III}Por-1. Porphyrin **2** was prepared according to a previously reported procedure.[26]
α-5,15-bis-({{2,2-(3,3-[2,2-(monocarboxylic acid)propane-1,3-diyl]-dibenzoyl-amido]-diphenyl)-10,20-bis-(4-hydroxyphenyl)-porphyrin (3). Compound **2** (0.39 mmol, 400 mg) was dissolved in 50 mL of DMF and heated at 115 °C. The reaction was monitored in every half an hour by TLC and MALDI. After 2h of heating the reaction was completed. After removal of DMF in the rotary evaporator at 60 °C, the product was separated by column chromatography eluted with 5% DCM-MeOH. The expected compound was obtained in 80% yield (305 mg). ^{1}H NMR (DMSO-d_6, 298 K, 500.13 MHz): δ 9.95 (2H, s, OH), 9.07 (2H, s, NHCO), 8.95 (2H, βpyr), 8.86 (2H, βpyr), 8.81 (4H, βpyr), 8.37 (2H, aro_9), 8.34 (2H, d, J = 7.49 Hz, $aro_{4'}$), 7.17 (4H, aro_8, $aro_{8'}$, aro_{11}, $aro_{11'}$), 7.07 (2H, d, J = 7.59 Hz, aro_6), 6.91 (2H, t, ^3J = 7.50 Hz, aro_5), 6.77 (2H, d, J = 7.59 Hz, aro_4), 4.94 (2H, s, aro_2), 2.28 (1H, CH_α), 1.38 (2H, $CH_{2\ bz(out)}$), 0.87 (2H, $CH_{2\ bz(in)}$), -2.79 (2H, NH_{int}). ^{13}C NMR (DMSO-d_6, 298 K, 125 MHz): δ 174.9, 166.2, 157.8, 139.3, 138.2, 136.2, 135.9, 135.8, 135.4, 135.3, 132.1, 129.7, 129.5, 129.3, 128.6, 128.5, 126.6, 125.7, 124.8, 124.2, 120.9, 120.2, 115.7, 114.4, 44.86, 36.28. ESI-HRMS: calcd m/z = 969.3395 $[M+H]^+$ for $C_{62}H_{45}N_6O_6$, found 969.3395, calcd m/z = 991.3214 $[M+Na]^+$ for $C_{62}H_{44}N_6O_6Na$, found 991.3211. UV-vis (DMF): λ/nm (10^{-3} ε, $dm^3\ mol^{-1}\ cm^{-1}$): 426 (346), 521 (26.6), 558 (19.6), 598 (14.2), 652 (13.4).

α-5,15-bis-({{2,2-(3,3-[2-(monocarboxylate)]-dibenzoyl-amido]-diphenyl)-10,20-bis-(4-hydroxyphenyl)-Bi(III)porphyrin (3Bi). Compound **3** (0.20 mmol, 200 mg) was dissolved in a mixture of DCM/MeOH (1:1, 50 mL), 2 equiv. of *N*,*N*-diisopropylethylamine were added to the stirring solution. Then 2 equiv. of $Bi(NO_3)_3.5H_2O$ (200 mg) were taken in MeOH (5 mL) and added to the solution. After 12 h of stirring at RT, solvents were removed under reduced pressure. The crude residue was purified by column chromatography eluted with 1% DCM/MeOH. The expected compound was obtained in 90% yield (217 mg). ^{1}H NMR (DMSO-d_6, 298 K, 500.13 MHz): δ 9.98 (2H, bs, OH), 9.48 (2H, s, NHCO), 9.24 (2H, d, J = 8.46 Hz, $aro_{2'}$), 9.17 (2H, d, J = 4.83 Hz, βpyr),

9.02 (2H, d, J = 4.45 Hz, βpyr), 8.99 (2H, d, J = 4.45 Hz, βpyr), 8.96 (2H, d, J = 4.45 Hz, βpyr), 8.13 (4H, bs, $aro_{5'}$, aro_9), 7.89 (2H, t, ^3J = 7.84 Hz, $aro_{3'}$), 7.68 (2H, d, J = 8.66 Hz, $aro_{9'}$), 7.63 (2H, t, ^3J = 7.63 Hz, $aro_{4'}$), 7.26 (2H, d, J = 7.75 Hz, aro_6), 7.23 (2H, d, J = 8.44 Hz, aro_8), 7.10 (2H, d, J = 8.44 Hz, $aro_{8'}$), 7.00 (2H, t, ^3J = 7.55 Hz, aro_5), 6.89 (2H, d, J = 7.55 Hz, aro_4), 5.45 (2H, s, aro_2), 2.30 (2H, d, J = 12.06 Hz, $CH_{2\ bz(out)}$), 1.79 (2H, m, $CH_{2\ bz(in)}$), 1.32 (1H, t, ^3J = 12.29 Hz, CH_α). ^{13}C NMR (DMSO-d_6, 298 K, 125 MHz): δ 173.8, 167.5, 157.8, 157.7, 150.9, 149.3, 149.2, 147.2, 141.3, 139.9, 136.0, 135.5, 134, 133.2, 132.7, 131.9, 131.8, 131.2, 130.8, 129.6, 128.1, 127.2, 126.2, 124.5, 123.7, 123, 120.1, 118.4, 114.5, 114, 55.7, 40.2. ESI-HRMS: calcd m/z = 1175.2964 $[M+H]^+$ for $C_{62}H_{42}N_6O_6Bi$, found 1175.2963, calcd m/z = 1197.2783 $[M+Na]^+$ for $C_{62}H_{41}N_6O_6BiNa$, found 1197.2768. UV-vis (DMF): λ/nm (% of absorbance): 403 (21%), 475 (100%), 614 (6.5%), 668 (8.8%).

α-5,15-bis-({{2,2-(3,3-[2-(monocarboxylate)]-dibenzoyl-amido]-diphenyl)-10,20-bis-(4-{3-bromopropoxyphenyl)-Bi(III)porphyrin (4). 300 mg (0.25 mmol, 1 equiv.) of porphyrin **3Bi** were dissolved in 100 mL of DMF and were taken in a dropping funnel. Then 50 equivalents of 1,3-dibromopropane (1.3 mL) were introduced into the round bottom flask along with 10 equiv. of activated K_2CO_3 (352 mg) into 20 mL of DMF. The diluted green porphyrin solution was added dropwise to the stirring solution of 1,3-dibromopropane. The solution was stirred for ~36 hours at RT under an argon atmosphere. The reaction was monitored by TLC and MALDI-TOF, and once complete, the solvent was removed under reduced pressure. The crude product was purified by column chromatography eluted with 0.4% DCM/MeOH. The desired compound was obtained in 55% yield (200 mg). ^{1}H NMR ($CDCl_3$, 298 K, 500.13 MHz,): δ 9.42 (2H, d, J = 4.74 Hz, βpyr), 9.33 (2H, d, J = 4.74 Hz, βpyr), 9.20 (6H, bs, βpyr, $aro_{2'}$), 8.39 (2H, s, NHCO), 8.15 (4H, bs, $aro_{5'}$, aro_9), 8.01 (2H, d, J = 8.27 Hz, $aro_{9'}$), 7.93 (2H, t, ^3J = 7.62 Hz, $aro_{3'}$), 7.61 (2H, t, ^3J = 7.73 Hz, $aro_{4'}$), 7.46 (2H, d, J = 7.73 Hz, aro_4), 7.32 (4H, bs, aro_9, $aro_{9'}$), 6.97 (2H, t, ^3J = 7.73 Hz, aro_5), 6.80 (2H, d, J = 7.73 Hz, aro_6), 5.55 (2H, s, aro_2), 4.45 & 4.41 (4H, 2t, ^3J = 5.69 Hz, alp_3, $alp_{3'}$), 3.79 (4H, alp_1, $alp_{1'}$), 2.53 (4H, alp_2, $alp_{2'}$), 2.29 (2H, d, J = 10.37 Hz, $CH_{2\ bz(out)}$), 1.81 (2H, $CH_{2\ bz(in)}$), 1.29 (1H, m, CH_α). ^{13}C NMR ($CDCl_3$, 298 K, 125 MHz,): δ 178.6, 166.3, 159.1, 158.9, 149.8, 149.7, 148.9, 146.9, 139.9, 139.7, 136.1, 135.6, 135.4, 134.8, 134.1, 133.7, 132.9, 132.8, 131.8, 131.5, 130.4, 130.1, 128.5, 126.6, 124.6, 122.9, 120.6, 117.1, 113.7, 113, 112.8, 65.7, 65.6, 54.8, 40.3, 32.5, 30.1. ESI-HRMS: calcd m/z = 1415.2113 $[M+H]^+$ for $C_{68}H_{52}N_6O_6{}^{79}Br_2Bi$, found 1415.2118, calcd m/z = 1370.2136 $[M-CO_2]^{+\cdot}$ for $C_{67}H_{51}N_6O_4{}^{79}Br_2Bi$, found 1370.2134. UV-vis (DCM): λ/nm (% of absorbance): 355 (25%), 478 (100%), 610 (4.3%), 660 (7.2%).

α-5,15-bis-({{2,2-(3,3-[2-(monocarboxylate)]-dibenzoyl-amido]-diphenyl)-10,20-bis-(4-{3-pyridiniumbromidepropoxyphenyl}-Bi(III)porphyrin (1Bi). 200 mg (0.14 mmol) of porphyrin **4** were dissolved in 50 mL of pyridine. Then the green solution was refluxed for 8 h, after what the

desired compound was precipitated from the pyridine solution. The compound was filtered by a filtrate paper and washed several times by cold DCM. Then the precipitated compound was dissolved in MeOH and the solvent was removed by rotary evaporator. The crude compound was purified by neutral Al_2O_3 using 30% MeOH in DCM. The expected compound was obtained in 85% yield (188 mg). ^{1}H NMR (CD_3OD, 298 K, 500.13 MHz,): δ 9.37 (2H, d, *J* = 4.69 Hz, βpyr), 9.30 (4H, βpyr), 9.17 (4H, βpyr, p_o), 9.11 (2H, d, *J* = 6.46 Hz, $p_{o'}$), 9.06 (2H, d, *J* = 8.68 Hz), 8.65 (2H, p_p, $p_{p'}$), 8.20 (6H, p_m, $p_{m'}$, $aro_{5'}$), 8.09 (2H, d, *J* = 7.85 Hz, aro_9), 7.99 (2H, d, *J* = 7.85 Hz, $aro_{9'}$), 7.93 (2H, t, ^3J = 8.39 Hz, $aro_{3'}$), 7.65 (2H, t, ^3J = 7.71 Hz, $aro_{4'}$), 6.86 (2H, d, *J* = 7.71 Hz, aro_4), 7.20 (4H, aro_8, $aro_{8'}$), 6.98 (2H, t, ^3J = 7.28 Hz, aro_5), 6.87 (2H, d, *J* = 7.71 Hz, aro_6), 5.41 (2H, s, aro_2), 5.01, 4.93 (4H, 2t, ^3J = 6.96 Hz, alp_3, $alp_{3'}$), 4.40 (4H, alp_1, $alp_{1'}$), 2.68 (4H, alp_2, $alp_{2'}$), 2.38 (2H, d, *J* = 11.90 Hz, $CH_{2\ bz(out)}$), 1.79 (2H, t, ^3J = 12.13 Hz, $CH_{2\ bz(in)}$), 1.43 (1H, t, ^3J = 12.07 Hz, CH_α). ^{13}C NMR (CD_3OD, 298 K, 125 MHz,): δ 180.1, 168.3, 158.6, 158.5, 149.4, 149.3, 148.7, 147.4, 145.7, 145.6, 145.1, 145, 140.2, 139.5, 136.1, 135.3, 135.1, 134.8, 134.2, 133.9, 133.7, 132.9, 132.4, 131.4, 131.3, 131.1, 129.5, 128.2, 128.1, 128, 125.7, 124.6, 124.3, 123.7, 123.2, 120.9, 117.6, 112.5, 64.9, 59.7, 59.6, 55.6, 39.6, 30.4, 30.3. ESI-HRMS: calcd m/z = 707.2253 $[M\text{-}2Br]^{++}$ for $C_{78}H_{61}N_8O_6Bi$, found 707.2257. UV-vis (DMF): λ/nm (% of absorbance): 403 (22%), 475 (100%), 612 (7.8%), 667 (9.9%).

α-5,15-bis-({{2,2-(3,3-[2-(monocarboxylic acid)]-dibenzoyl-amido]-diphenyl)-10,20-bis-(4-{3-pyridiniumbromidepropoxyphenyl }}-porphyrin (1). 200 mg of porphyrin **1Bi** (0.12 mmol) were dissolved in 50 mL of THF/MeOH (1:1). Then 1 mL of concentrated hydrobromic acid was added to the green solution and stirred for 12h at RT, after that the solution was concentrated under reduced pressure. The residue was washed by H_2O several times using a filtrate paper. Then the precipitated compound was dissolved by MeOH and the solvent was removed by rotary evaporator. The desired compound was purified by neutral Al_2O_3 using 1% AcOH in a mixture DCM/MeOH (1/1). The expected compound was obtained in 86% yield (150 mg). ^{1}H NMR (DMSO-d_6, 298 K, 500.13 MHz,): δ 9.37 (4H, P_o, $P_{o'}$), 9.17 (2H, s, NHCO), 8.87 (4H, bs, βpyr), 8.82 (2H, βpyr), 8.70 (4H, βpyr, P_p, $P_{p'}$), 8.45 (2H, d, *J* = 7.17 Hz, aro_9), 8.36 (1H, s, CO_2H), 8.26 (8H, P_m, $P_{m'}$, $aro_{2'}$, $aro_{5'}$), 8.05 (2H, d, *J* = 7.87 Hz, $aro_{9'}$), 7.92 (4H, aro_{12}, $aro_{12'}$, $aro_{3'}$), 7.73 (2H, t, ^3J = 7.45 Hz, $aro_{4'}$), 7.19 (4H, aro_9, $aro_{9'}$, aro_{11}, $aro_{11'}$), 7.04 (2H, d, *J* = 7.91 Hz, aro_4), 6.89 (2H, t, ^3J = 7.73 Hz, aro_5), 6.79 (2H, d, *J* = 7.73 Hz, aro_6), 5.01 (4H, alp_3, alp3'), 4.93 (2H, s, aro_2), 4.41 (4H, alp_1, $alp_{1'}$), 2.62 (4H, alp_2, $alp_{2'}$), 2.36 (1H, CH_α), 1.44 (2H, $CH_{2\ bz(out)}$), 0.85 (2H, $CH_{2\ bz(in)}$), -2.84 (2H, s, NH_{int}). ^{13}C NMR (DMSO-d_6, 298 K, 500.13 MHz,): δ 166.3, 158.3, 146.1, 145.7, 139.2, 138.2, 135.9, 135.7, 135.6, 135.4, 134.1, 134, 129.8, 129.4, 128.5, 126.7, 125.7, 124.9, 124.7, 120.2, 119, 116.1, 113.3, 79.7, 65.7, 59.5, 36.2, 30.6. ESI-HRMS: calcd m/z = 604.2468 $[M\text{-}2Br]^{++}$ for $C_{78}H_{64}N_8O_6$, found 604.2473UV-vis (DMF): λ/nm (10^{-3} ε, dm^3 mol^{-1} cm^{-1}): 425 (360), 520 (18), 557 (10), 596 (7), 653 (5).

α-5,15-bis-({{2,2-(3,3-[2-(monocarboxylate)]-dibenzoyl-amido]-diphenyl)-10,20-bis-(4-{3-pyridiniumbromidepropoxyphenyl})-Fe(III)porphyrin (Fe^{III}Por-1). 120 mg (0.08 mmol) of porphyrin **1** were dissolved in 20 mL of dry, degassed THF along with 5 mL of MeOH in the glove box. Then excess amount of $FeBr_2$ was added into the solution along with 50 μL of 2,6-lutidine acting as a base. The solution was stirred for ~24 hours at RT under an argon atmosphere. The reaction was monitored by UV-visible spectroscopy. After completion of the reaction the compound was removed from the glove box and dried by the rotary evaporator. The crude product was washed by acidic water and then purified by column chromatography (using Al_2O_3) eluted with 40% MeOH/DCM. The desired compound was obtained in 90% yield (112 mg). ESI-HRMS: calcd m/z = 630.7026 $[M]^{++}$ for $C_{78}H_{61}N_8O_6{}^{56}Fe$, found 630.7026. UV-vis (DMF): λ/nm (% of absorbance): 419 (100%), 511 (8%).

Complexation of Fe^{III}PorCD-1 with Py3OCD. For the titration experiments, the stock solutions of **Fe^{III}PorCD-1** (1.0 mM) and **Py3OCD** (1.0 mM) were independently prepared in pure water. The solutions were appropriately diluted in a 1-cm cuvette and then the UV-vis spectrum was recorded stepwise. For the ESI-TOF-MS analysis, **Fe^{III}PorCD-1** (1.0 mM) and **Py3OCD** (1.0 mM) were equimolarly mixed in pure water and infused into the ion source of the instrument using a syringe pump.

Preparation of O_2 and CO complexes. Fe^{III}PorCD-1 (a 1.0:1.2 mixture of **Fe^{III}Por-1** and **Py3OCD**) in 0.05 M phosphate buffer solution at pH 7.0 was reduced with $Na_2S_2O_4$. Excess $Na_2S_2O_4$ and its oxidized byproducts were removed by passing the solution through a HiTrap desalting column (Sephadex G25, GE Healthcare Life Sciences). During the column treatment, the complex became its O_2 adduct by capturing atmospheric O_2. The CO–complex was prepared by introducing CO gas into the solution of deoxy or O_2 complex.

Determination of the gas binding affinities. For determination of $P_{1/2}{}^{CO}$, the CO/N_2 mixed gas with various CO partial pressures (P^{CO}) was introduced into the phosphate buffer solution (0.05 M, pH 7.0) at 25˚C. After 15 min, the stock solution of **Fe^{II}PorCD-1** was added quickly, and the gas bubbling was continued for another 3 min. For determination of $P_{1/2}{}^{O2}$, the $CO/N_2/O_2$ mixed gas with various CO partial pressures (P^{CO}) was bubbled into the phosphate buffer solution (0.05 M, pH 7.0) at 25˚C. After bubbling for 15 min, the solution of **O$_2$–Fe^{II}PorCD-1** was added quickly, and the gas bubbling was continued for another 3 min. The absorbance change was plotted against P^{CO}. The curve fitting analysis was conducted based on eq 5;[14,21,29]

$$\Delta Abs = \frac{\Delta\varepsilon\,[\mathbf{Fe^{II}PorCD-1}]_t \cdot P^{CO}}{P^{CO} + P_{1/2}^{CO}}$$

(5)

where ΔAbs is the absorbance change of **Fe^{II}PorCD-1** (435 nm). $\Delta\varepsilon$ is the difference in the extinction coefficient between **Fe^{II}PorCD-1** and **CO–Fe^{II}PorCD-1** at 435 nm. [**Fe^{II}PorCD-1**]$_t$ is the total concentration of the iron porphyrin.

The M value ($M = P_{1/2}^{O2} / P_{1/2}^{CO}$) was determined based on the gas titration experiment for **Fe^{II}PorCD-1** (and its related compounds) using the CO/O_2 mixed gas. Upon increasing the CO partial pressure of the mixed gas, **O$_2$-Fe^{II}PorCD-1** was converted to **CO-Fe^{II}PorCD-1**. The absorbance change was analyzed by using the same equation as eq 5 to determine the CO partial pressure at which the concentrations of **O$_2$-** and **CO-Fe^{II}PorCD-1** were equal. The M value was determined by the ratio of the CO and O_2 partial pressures (P^{O2}/P^{CO}) at which **O$_2$-** and **CO-FePorCD-1** were equally contained (see eq 2). The partial pressure of N_2 contained in the diluted CO gas was taken into calculation. The $P_{1/2}^{O2}$ value was determined by eq 2.

Laser flash photolysis. The pseudo first-order rate constants (k_{obs}^{L}, L = CO or O_2) of each compound were measured by laser-flash photolysis.[14] The solution of O_2- and CO-**Fe^{II}PorCD-1** and its related compounds (**Fe^{II}PorCD-1** and **hemoCD3**) were prepared by the same procedure as described above. Rebinding of O_2 and CO was monitored by following the changes in the absorbances at the wavelength indicated in the raw data after excitation by a laser flash (λ_{ex} = 532 nm, 5 ns pulse) at pH 7.0 and 25°C. The O_2 and CO partial pressures were regulated by introducing the O_2/N_2 and CO/N_2 mixed gases into the solution 15 min before the measurements. The k_{obs}^{L} for O_2 and CO association were determined by curve fitting analysis using the nonlinear least-squares method. The k_{obs}^{L} were plotted against [O_2] and [CO], and the k_{on}^{L} for O_2 and CO were determined by the slopes of the linear regression lines according to eq 4. Since the intercepts of the linear regression lines were too small to determine k_{off}^{L}, the k_{off}^{L} values were calculated from eq 6:[29]

$$K^{L} = (C^{L}P_{1/2}^{L})^{-1} = k_{on}^{L}/k_{off}^{L} \quad (6)$$

where C^L is the solubility of O_2 or CO in water at 25 °C (C^{O2} = 1.67 x 10^{-6} M Torr^{-1}, C^{CO} = 1.26 x 10^{-6} M Torr^{-1}).[36]

IR spectroscopy. Aqueous solutions of **CO-Fe^{II}PorCD-1** and its related compounds were prepared by addition of CO and $Na_2S_2O_4$ to the corresponding ferric complexes in 0.05 M phosphate buffer at pH 7.0. The concentration of the complexes was (1–2) × 10^{-3} M. The solution (50 μL) of the CO–complex was loaded into a demountable FTIR liquid cell with CaF_2 plate (PIKE Technologies). The IR spectra were recorded by Shimadzu IR Prestige-21. The CO bond stretching was detected after the subtraction of the control spectrum (buffer) from the original data.

Molecular mechanics calculations. Molecular mechanics calculation of **CO-Fe^{II}PorCD-1** was performed using CONFLEX/MM3 (extensive search) parameters in Scigress version 2.2.1 software program (Fujitsu).

Acknowledgments

We thank Prof. Shun Hirota and Dr. Satoru Nakashima (NAIST) for their helpful discussion on the vibrational spectroscopy. This work was financially supported by JSPS KAKENHI Grant Number JP18KK0156. The authors also gratefully acknowledge the International Research Project SUPRHEME from the CNRS and the Universities of Rennes and Strasbourg.

Associated content: Supporting information available: CIF files, NMR, HRMS, and UV-vis data for new synthesized compounds and supramolecular complexes.

References

(1) Perutz, M. F. Mechanisms regulating the reactions of human hemoglobin with oxygen and carbon monoxide. *Annu. Rev. Physiol.* **1990**, *52*, 1–25.

(2) Jameson, G. B.; Ibers, J. A. Biological and synthetic dioxygen carriers. In *Bioinorganic Chemistry*; Bertini, I., Gray, H. B., Lippard, S. J., Valentine, J. S., Eds.; University Science Books: Mill Valley, CA, **1994**; pp 167–251.

(3) Springer, B. A.; Sligar, S. G.; Olson, J. S.; Phillips. Jr, G. N. Mechanisms of ligand recognition in myoglobin. *Chem. Rev.* **1994**, *94*, 699–714.

(4) Collman, J. P.; Boulatov, R.; Sunderland, C. J.; Fu, L. Functional analogues of cytochrome *c* oxidase, myoglobin, and hemoglobin. *Chem. Rev.* **2004**, *104*, 561–588.

(5) Momenteau, M.; Reed, CA. Synthetic heme dioxygen complexes. *Chem. Rev*. **1994**, *94*, 659–698.

(6) Kossanyi, A.; Tani, F.; Nakamura, N.; Naruta, Y. Properties of a binaphthyl-bridged porphyrin – iron complex bearing hydroxy groups inside its cavity. *Chem. Eur. J.* **2001**, *7*, 2862–2872.

(7) Tani, F.; Matsu-ura, M.; Ariyama, K.; Setoyama, T.; Shimada, T.; Kobayashi, S.; Hayashi, T.; Matsuo, T.; Hisaeda, Y.; Naruta, Y. Iron twin-coronet porphyrins as models of myoglobin and hemoglobin: amphibious electrostatic effects of overhanging hydroxyl groups for successful CO/O_2 discrimination. *Chem. Eur. J.* **2003**, *9*, 862–870.

(8) Shikama, K. The molecular mechanism of autoxidation for myoglobin and hemoglobin: A venerable puzzle. *Chem. Rev.* **1998**, *98*, 1357–1374.

(9) Shikama, K. Stability properties of dioxygen-iron(II) porphyrins: an overview from simple complexes to myoglobin. *Coord. Chem. Rev.* **1988***, 83*, 73–91.

(10) Kano, K.; Tanaka, N.; Minamizono, H.; Kawakita, Y. Tetraarylporphyrins as probes for studying mechanism of inclusion-complex formation of cyclodextrins. Effect of microscopic environment on inclusion of ionic guests. *Chem. Lett.* **1996**, 25, 925–926.

(11) Kano, K.; Nishiyabu, R.; Asada, T.; Kuroda, Y. Static and dynamic behavior of 2:1 inclusion complexes of cyclodextrins and charged porphyrins in aqueous organic media. *J. Am. Chem. Soc.* **2002**, *124*, 9937–9944.

(12) Kano, K.; Kitagishi, H.; Tamara, S.; Yamada, A. Anion binding to a ferric porphyrin complexed with per-*O*-methylated β-cyclodextrin in aqueous solution. *J. Am. Chem. Soc.* **2004**, *126*, 15202–15210.

(13) Kano, K.; Kitagishi, H.; Kodera, M.; Hirota, S. Dioxygen binding to a simple myoglobin model in aqueous solution. *Angew. Chem. Int. Ed.* **2005**, *44*, 435–438.

(14) Kano, K.; Kitagishi, H.; Dagallier, C.; Kodera, M.; Matsuo, T.; Hayashi, T.; Hisaeda, Y.; Hirota, S. Iron porphyrin-cyclodextrin supramolecular complex as a functional model of myoglobin in aqueous solution. *Inorg. Chem.* **2006**, *45*, 4448–4460.

(15) Kitagishi, H.; Kano, K. Synthetic heme protein models that function in aqueous solution. *Chem. Commun.* **2021**, *57*, 148–173.

(16) Watanabe, K.; Kitagishi, H.; Kano, K. Supramolecular iron porphyrin/cyclodextrin dimer complex that mimics the functions of hemoglobin and methemoglobin. *Angew. Chem. Int. Ed.* **2013**, *52*, 6894–6897.

(17) Kitagishi, H.; Mao, Q.; Kitamura, N.; Kita, T. HemoCD as a totally synthetic artificial oxygen carrier: improvements in the synthesis and O_2/CO discrimination. *Artif. Organs*. **2017**, *41*, 372–380.

(18) Sugiyasu, K.; Ogi, S.; Takeuchi, M. Strapped porphyrin-based polymeric systems. *Polymer J.* **2014**, *46*, 674–681.

(19) Wolf, M.; Ogawa, A.; Bechtold, M.; Vonesch, M.; Wytko, J. A.; Oohora, K.; Campidelli, S.; Hayashi, T.; Guldi, D. M.; Weiss, J. Light triggers molecular shuttling in rotaxanes: control over proximity and charge recombination, *Chem. Sci.* **2019**, *10*, 3846–3853.

(20) Balieu, S.; Hijazi, I.; Motreff, N.; Lachaud, F.; Even-Hernandez, P.; Boitrel, B. Steric decompression of picket-strapped porphyrins for the synthesis of side-differentiated chelates. *Org. Lett.* **2010**, *12*, 8–11.

(21) Collman, J. P.; Zhang, X. M.; Wong, K.; Brauman, J. I. Dioxygen binding in iron and cobalt basket porphyrins. *J. Am. Chem. Soc.* **1994**, *116*, 6245–6251.

(22) Ruzié, C.; Even, P.; Ricard, D.; Roisnel, T.; Boitrel, B. O_2 and CO binding to tetraaza-Tripodal-capped iron(II) porphyrins. *Inorg. Chem.* **2006**, *45*, 1338−1348.

(23) Boitrel, B.; Le Gac, S. Stabilization of synthetic heme-superoxo complexes by hydrogen bonding: a still on-going quest. *New. J. Chem.* **2018**, *42*, 7516–7521.

(24) Hijazi, I.; Roisnel, T.; Fourmigué, M.; Weiss, J.; Boitrel, B. Coordination studies of bis-strapped-hanging-carboxylate porphyrins. X-ray characterization of a five-coordinate iron(II) complex with a built-in axial base. *Inorg. Chem.* **2010**, *49*, 3098–3100.

(25) Boitrel, B.; Hijazi, I.; Roisnel, T.; Oohora, K.; Hayashi, T. Iron-strapped porphyrins with carboxylic acid groups hanging over the coordination site: synthesis, x-ray characterization, and dioxygen binding. *Inorg. Chem.* **2017**, *56*, 7373–7383.

(26) Hanana, M.; Arcostanzo, H.; Das, P. K.; Bouget, M.; Le Gac, S.; Okuno, H.; Cornut, R.; Jousselme, B.; Dorcet, V.; Boitrel, B.; Campidelli, S. Synergic effect on oxygen reduction reaction of strapped iron porphyrins polymerized around carbon nanotubes. *New. J. Chem.* **2018**, *42*, 19749–19754.

(27) Boitrel, B.; Bouget, M.; Das, P. K.; Le Gac, S.; Roisnel, T.; Hanana, M.; Arcostanzo, H.; Cornut, R.; Jousselme, B.; Campidelli, S. Oxygen reduction reaction catalyzed by overhanging carboxylic acid strapped porphyrins adsorbed on carbon nanotubes. *J. Porphyrins Phthalocyanines* **2020**, 24, 675684.

(28) Le Gac, S.; Fusaro, L.; Roisnel, T.; Boitrel, B. Heterobimetallic porphyrin complexes displaying triple Dynamics: coupled metal motions controlled by constitutional evolution. *J. Am. Chem. Soc.* **2014**, 136, 6698–6715.

(29) Collman, J. P.; Brauman, J. I.; Doxsee, K. M.; Sessler, J. L.; Morris, R. M.; Gibson, Q. H. Effect of axial base on dioxygen and carbon monoxide affinities of iron(II) porphyrins. Imidazole vs. pyridine. *Inorg. Chem.* **1983**, *22*, 1427–1432.

(30) Sato, H.; Watanabe, M.; Hisaeda, Y.; Hayashi, T. Unusual ligand discrimination by a myoglobin reconstituted with a hydrophobic domain-linked heme. *J. Am. Chem. Soc.* **2005**, *127*, 56-57.

(31) Matsuo, T.; Dejima, H.; Hirota, S.; Murata, D.; Sato, H.; Ikegami, T.; Hori, H.; Hisaeda, Y.;

Hayashi, T. Ligand binding properties of myoglobin reconstituted with iron porphycene: Unusual O_2 binding selectivity against CO binding. *J. Am. Chem. Soc.* **2004**, *126*, 16007-16017.

(32) Li, T.; Quillin, M. L.; Phillips, Jr, G. N.; Olson, J. S. Structural determinants of the stretching frequency of CO bound to myoglobin. *Biochemistry* **1994**, *33*, 1433–1446.

(33) Yuan, X.; Spiro, T. G. Is bound carbonyl linear or bent in heme proteins? Evidence from resonance Raman and infrared spectroscopic data. *J. Am. Chem. Soc.* **1988**, *110*, 6024–6033.

(34) Matsu-ura, M., Tani, F.; Naruta, Y. Formation and characterization of carbon monoxide adducts of iron "Twin Coronet" porphyrins. extremely low CO affinity and a strong negative polar effect on bound CO. *J. Am. Chem. Soc.* **2002**, *124*, 1941-1950.

(35) Mao, Q.; Kawaguchi, A. T.; Mizobata, S.; Motterlini, R.; Foresti, R.; Kitagishi, H. Sensitive quantification of carbon monoxide (CO) *in vivo* reveals a protective role of circulating hemoglobin in CO intoxication. *Commun. Biol.* **2021**, 4: 425.

(36) The hydrophobic nature of CO is evidenced by the much larger solubility of CO gas in organic solvent than in water; see Wilhelm, E.; Battino, R.; Wilcock, R. J. Low-pressure solubility of gases in liquid water. *Chem. Rev.* **1977**, *77*, 219–262.

(37) Chang, C. K.; Liang, Y.; Aviles, G.; Peng, S.-M. Conformational control of intramolecular hydrogen bonding in heme models: maximal Co^{II}–O_2 binding in a c-clamp porphyrin. *J. Am. Chem. Soc.* **1995**, *117*, 4191–4192.

(38) Nishimura, R.; Shibata, T.; Ishigami, I.; Ogura, T.; Tai, H.; Nagao, S.; Matsuo, T.; Hirota, S.; Shoji, O.; Watanabe, Y.; Imai, K.; Neya, S.; Suzuki, A.; Yamamoto, Y. Electronic control of discrimination between O_2 and CO in myoglobin lacking the distal histidine residue. *Inorg. Chem*. **2014**, *53*, 1091−1099.

(39) Nishimura, R.; Matsumoto, D.; Shibata, T.; Yanagisawa, S.; Ogura, T.; Tai, H.; Matsuo, T.; Hirota, S.; Neya, S.; Suzuki, A.; Yamamoto, Y. Electronic control of ligand-binding preference of a myoglobin mutant. *Inorg. Chem.* **2014**, *53*, 9156–9165.

(40) Watanabe, M.; Kanai, Y.; Nakamura, S.; Nishimura, R.; Shibata, T.; Momotake, S.; Ogura, T.; Matsuo, T.; Hirota, S.; Neya, S.; Suzuki, A.; Yamamoto, Y. Synergistic effect of distal polar interactions in myoglobin and their structural consequences. *Inorg. Chem.* **2018**, *57*, 14269–14279.

(41) During the pH titration experiment, the absorbances of the **Fe^{III}PorCD-1** complex tended to significantly decrease outside the pH range 4-10, probably due to self-aggregated species. Therefore, the pK_a value for the overhanging COOH could not be determined correctly.

(42) Motoo, Y. Dissociation constants of some carboxylic acids in mixed aqueous solvents. *Bull. Chem. Soc. Jpn.* **1959**, 35, 429–432.

(43) Bashford, D.; Karplus, M. pK_a's of ionizable groups in proteins: atomic detail from a continuum electrostatic model. *Biochemistry*. **1990**, *29*, 10219–10225.

(44) Ghosh, I.; Nau, W. M. The strategic use of supramolecular pK_a shifts to enhance the bioavailability of drugs. *Adv. Drug Deliv. Rev*. **2012**, *64*, 764–783.

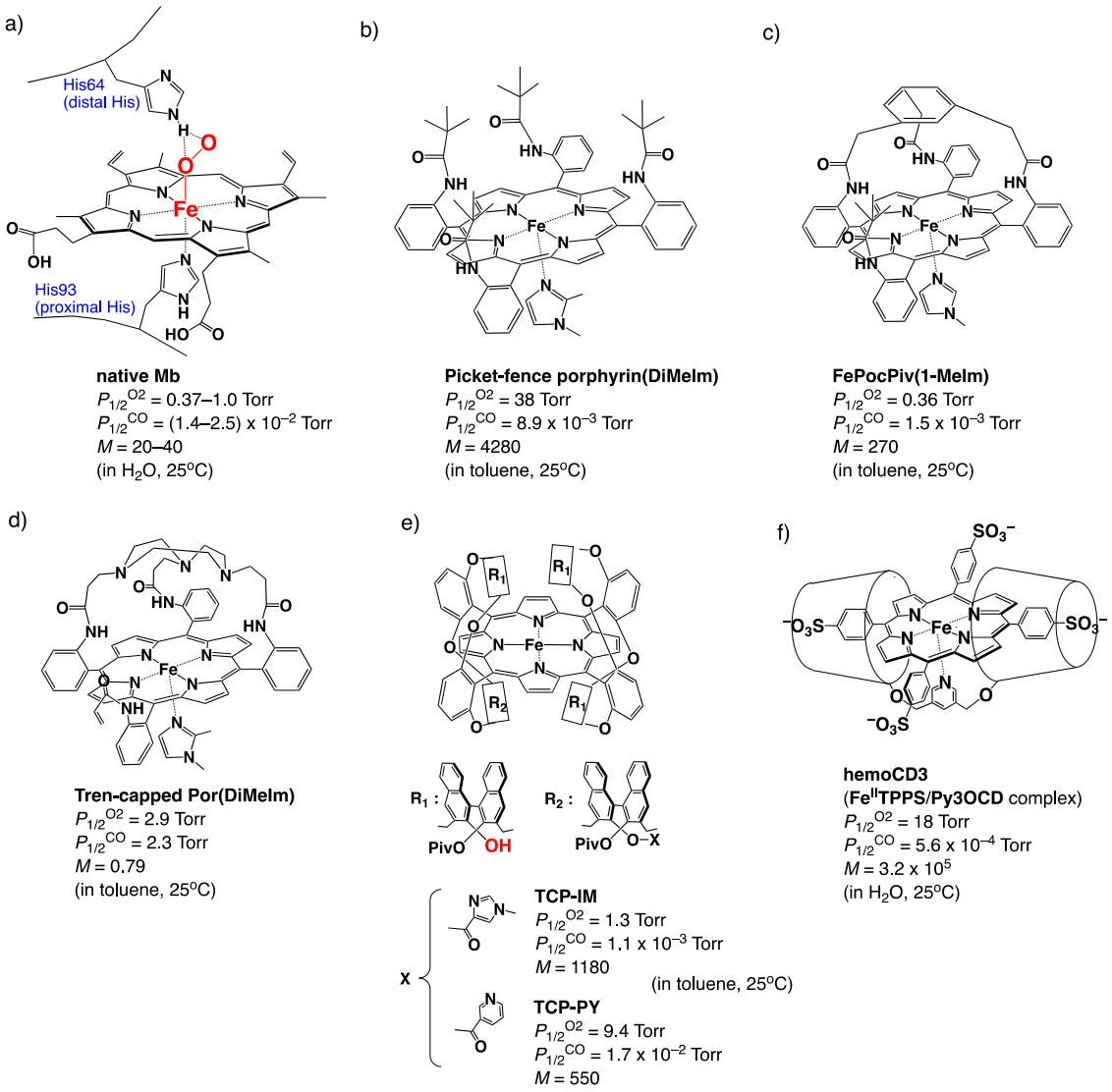

Figure 1. O_2 and CO binding affinities ($P_{1/2}^{O2}$ and $P_{1/2}^{CO}$) and selectivity values ($M = P_{1/2}^{O2}/P_{1/2}^{CO}$) of native myoglobin (a) and its synthetic model compounds (b-f).[4,7,16]

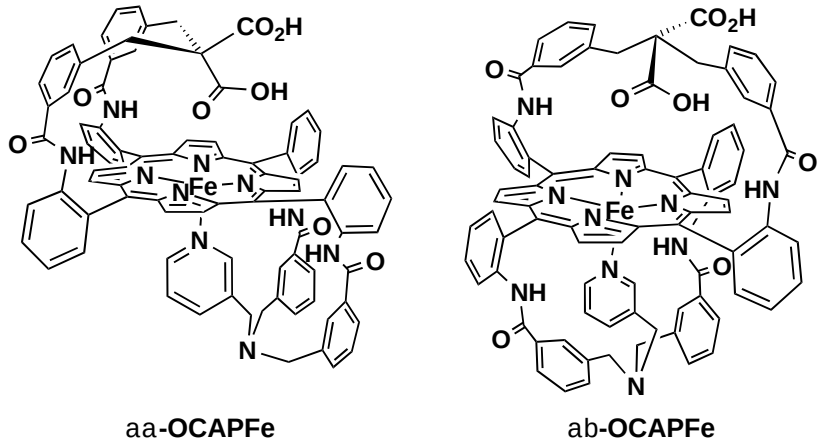

Figure 2. Synthetic Mb model compounds with overhanging carboxylic acids.[25]

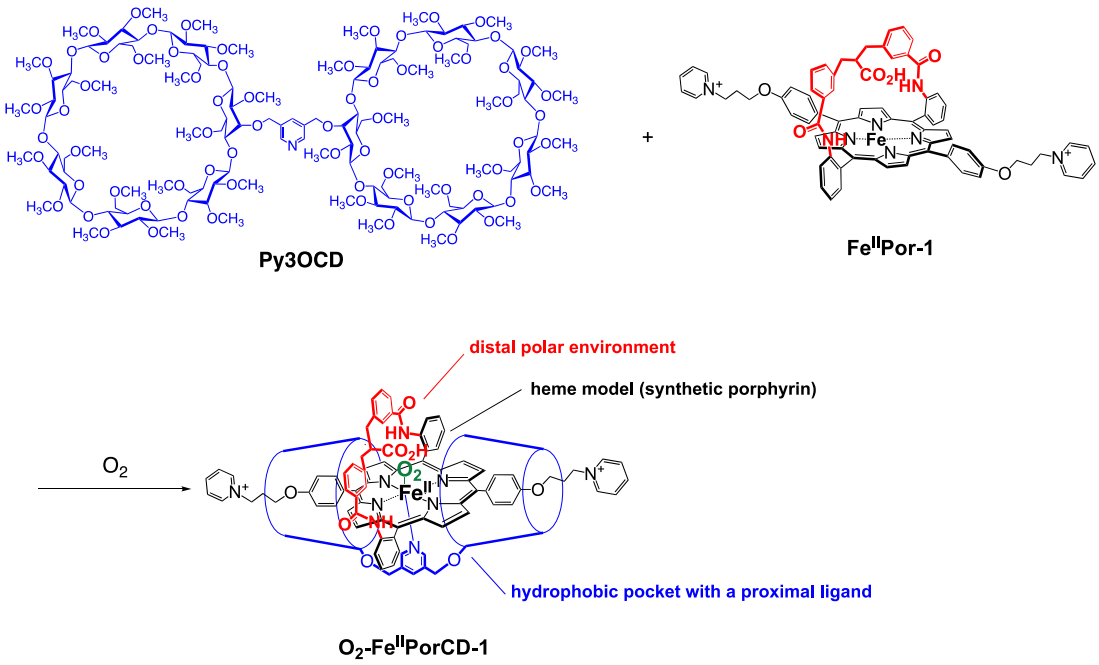

Figure 3. A new supramolecular Mb model that functions in aqueous solution. The model compound (**O_2-Fe^{II}PorCD-1**) has a Mb-like hydrophobic pocket and both proximal and distal functionalities, respectively provided by per-*O*-methyl-β-cyclodextrin dimer with a pyridine linker (**Py3OCD**) and the strapped porphyrin with an overhanging carboxylic acid group (**Fe^{II}Por-1**).

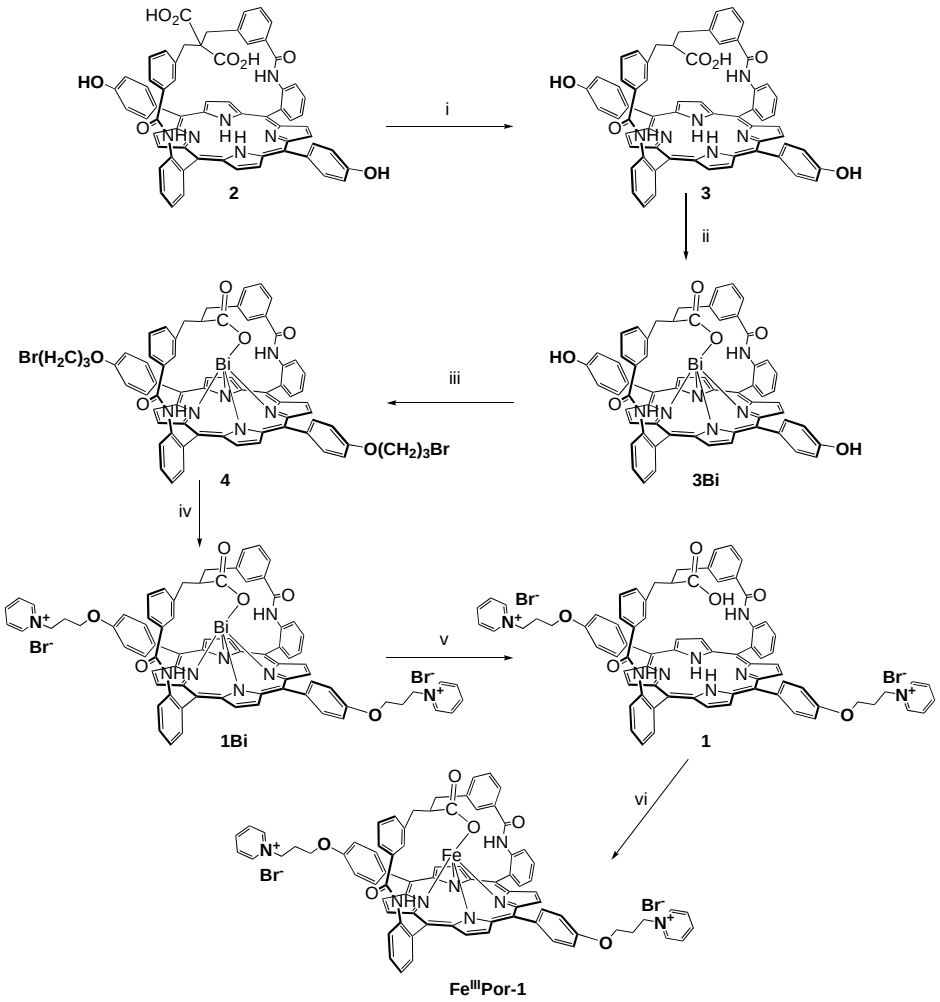

Scheme 1. Synthetic route to **Fe^{III}Por-1**. Reagents and conditions. (i) DMF, 115 °C, 2h, 80%; (ii) $Bi(NO_3)_3$ (2 equiv), DIPEA, (2 equiv), DCM/MeOH (1:1), 12 h, RT, 90%; (iii) 1,3-dibromopropane (50 equiv), K_2CO_3 (10 equiv), DMF, 36 h, RT, 55%; (iv) reflux pyridine, 8 h, 85%; (v) HBr, THF/MeOH (1:1), 12 h, RT, 86 %; (vi) 2,6-lutidine, $FeBr_2$, THF, 24 h, RT, 90%.

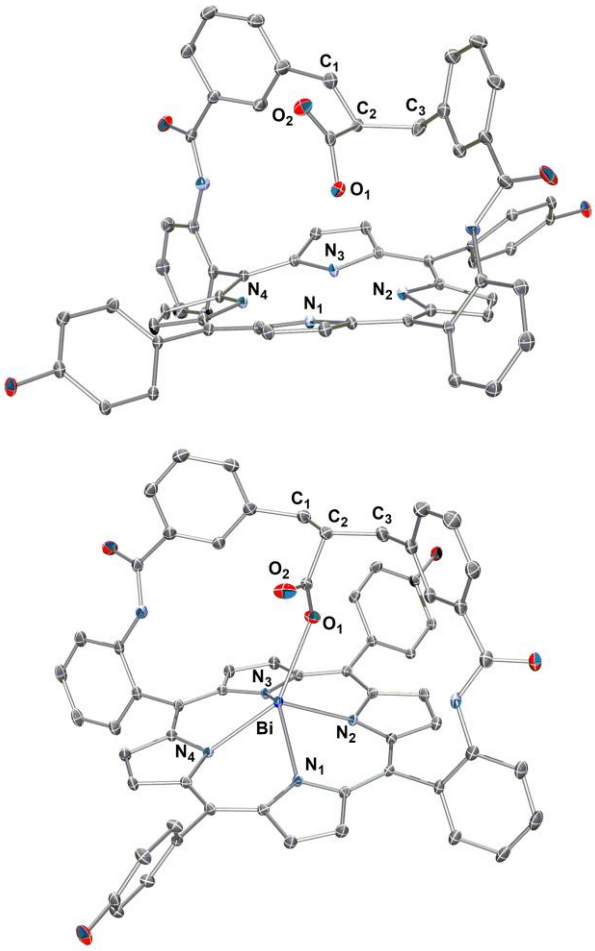

Figure 4. X-ray crystal structures of the strapped porphyrins **3** (top, CCDC 2078099) and **3Bi** (bottom, CCDC 2078100). Selected distances (Å) **3**: 4N centroid-O1 2.823, **3Bi**: O1-Bi 2.549, N1-Bi 2.399, N2-Bi 2.282, N3-Bi 2.286, N4-Bi 2.392.

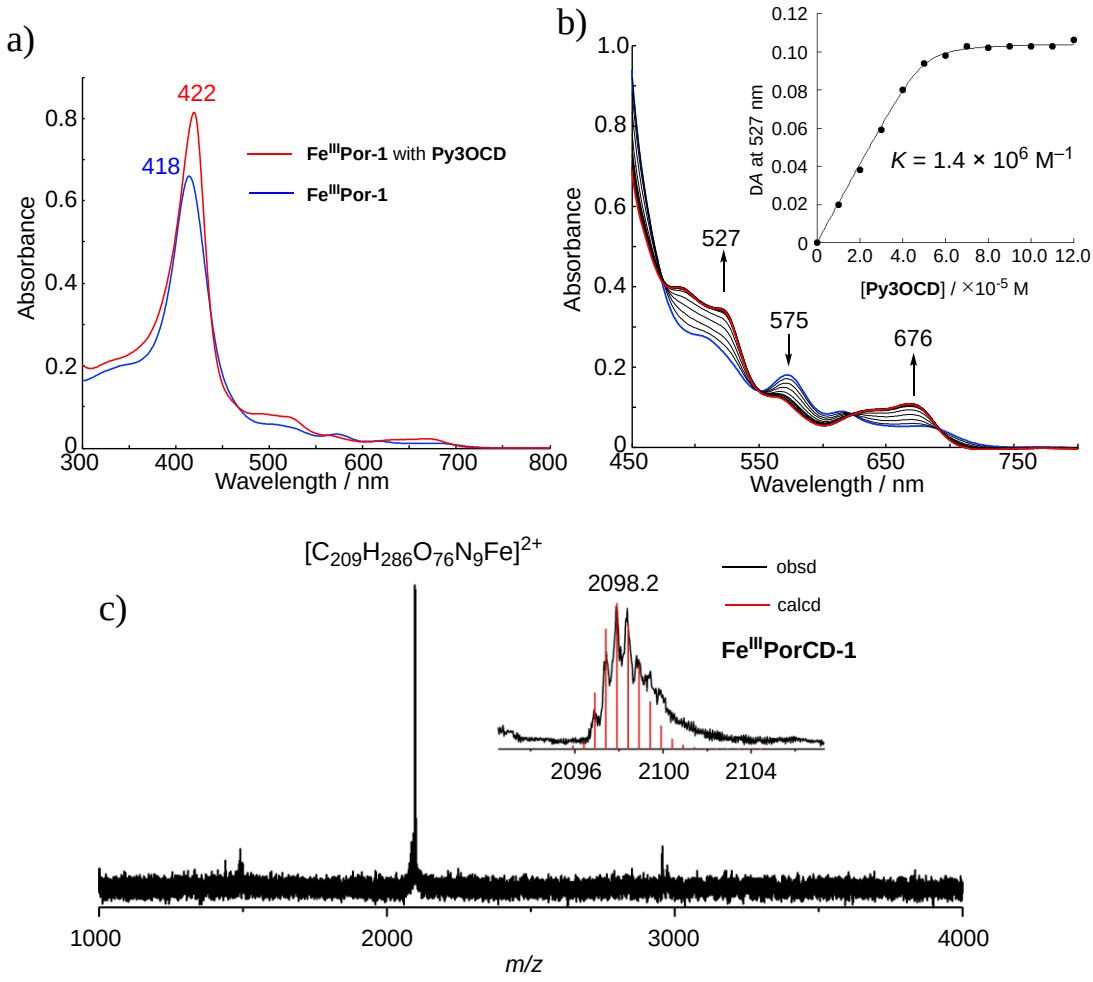

Figure 5. Supramolecular host-guest interaction between **Fe^{III}Por-1** and **Py3OCD**. (a) UV-vis spectra of **Fe^{III}Por-1** without and with **Py3OCD**, and (b) UV-vis spectral change of **Fe^{III}PorCD-1** as a function of [**Py3OCD**] in aqueous solution at 25°C. The inset in (b) shows a titration curve. The solid line represents the best-fit to the theoretical curve based on the 1:1 complexation. (c) ESI-MS of the 1:1 mixture of **Fe^{III}Por-1** and **Py3OCD** in water. The inset shows the simulated isotope distribution patterns for the complex **Fe^{III}PorCD-1**, calcd for m/z = 2098.2 $[C_{209}H_{286}O_{76}N_9Fe]^{2+}$, found 2098.2.

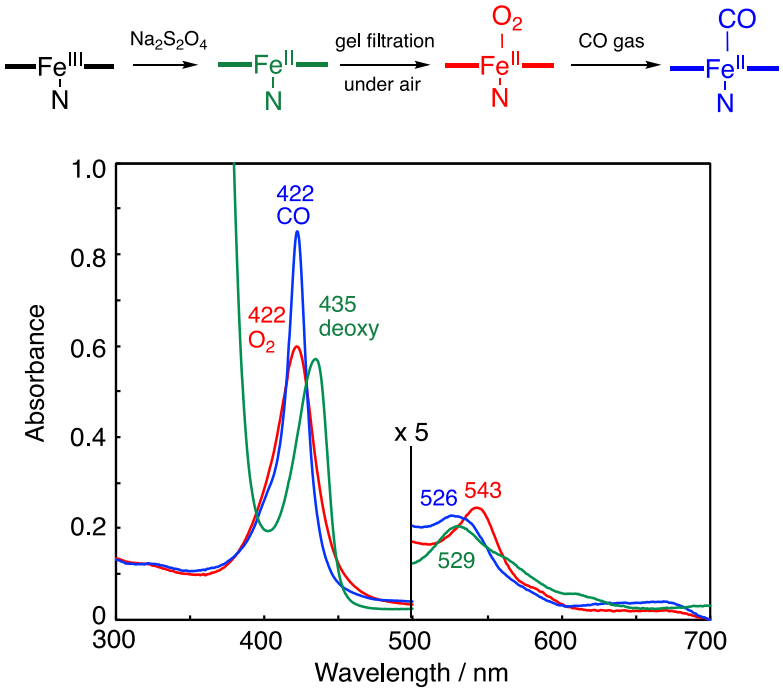

Figure 6. UV-vis spectra of **Fe^{II}PorCD-1** in the deoxy form and its O_2 and CO complexes in 0.05 M phosphate buffer at pH 7.0 and 25°C. The deoxy complex was prepared by adding excess sodium dithionite to a solution of **Fe^{III}PorCD-1**. The O_2 complex was then obtained after removing excess sodium dithionite by gel filtration under aerobic conditions. The solution was then bubbled with CO gas to obtain the CO complex.

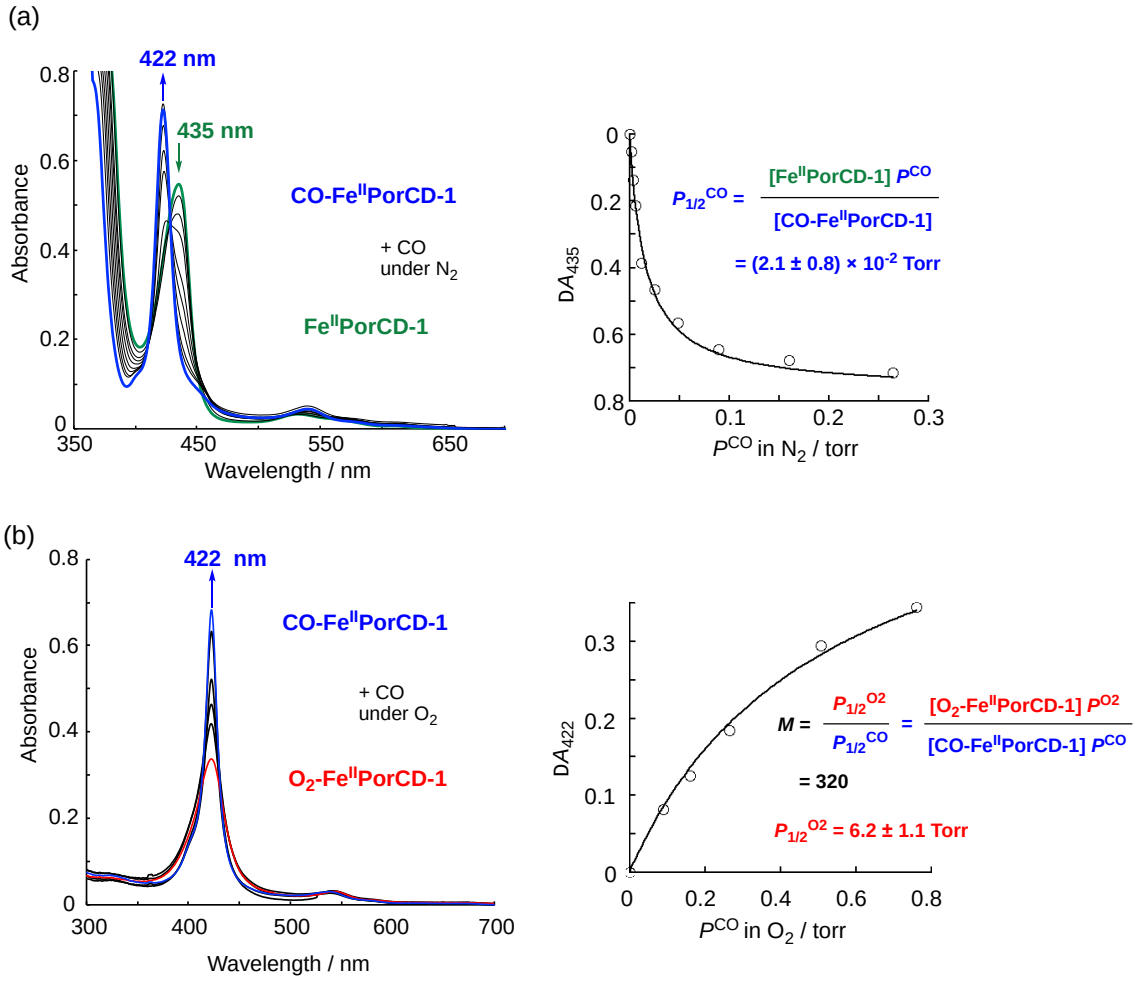

Figure 7. Determination of CO and O_2 affinities. (a,b) UV-vis spectral change of **Fe^{II}PorCD-1** as a function of partial pressures of CO (P^{CO}) under N_2 (a) and O_2 atmospheres (b) in 0.05 M phosphate buffer solution at pH 7.0 and 25°C. The spectra in (a) were measured in the presence of excess sodium dithionite to obtain the deoxy complex. The insets show the changes in absorbance at 435 nm as a function of P^{CO}. The solid lines represent theoretical curves to determine $P_{1/2}{}^{CO}$ and M values (see eqs (1) and (2) in the text).

Table 1. CO and O_2 binding affinities ($P_{1/2}^{CO}$, $P_{1/2}^{O2}$) and O_2/CO selectivity (M value) of native Mb and related model compounds.

	$P_{1/2}^{CO}$ (Torr)	$P_{1/2}^{O2}$ (Torr)	$P_{1/2}^{O2}/P_{1/2}^{CO}$ (= M)	Conditions
Mb [a]	(1.4–2.5)	0.37–1	20–40	H_2O, 25°C
Hb-R state [a]	1.4×10^{-3}	0.22	150	H_2O, 25°C
Picket-fence Por (DiMeIm) [a]	8.9×10^{-3}	38	4280	Toluene, 25°C
FePocPiv (1-MeIm) [a]	1.5×10^{-3}	0.36	270	Toluene, 25°C
Tren-capped Por (DiMeIm) [a]	2.9	2.3	0.79	Toluene, 25°C
TCP-IM [b]	1.1×10^{-3}	1.3	1180	Toluene, 25°C
TCP-PY [b]	1.7×10^{-2}	9.4	550	Toluene, 25°C
αα-OCAPFe [c]		< 9.3		Benzene, 25°C
αβ-OCAPFe [c]		10^{-3}		Benzene, 25°C
hemoCD3 [d]	5.6×10^{-4}	18	3.2×10^{4}	H_2O, 25 °C
Fe^{II}PorCD-1 [d]	2.1×10^{-2}	6.3	320	H_2O, 25 °C
Fe^{II}PorCD-2 [d]	3.8×10^{-4}	8.0	2.1×10^{4}	H_2O, 25 °C

[a] Ref (4), [b] Ref (7), [c] Ref (25), [d] This work

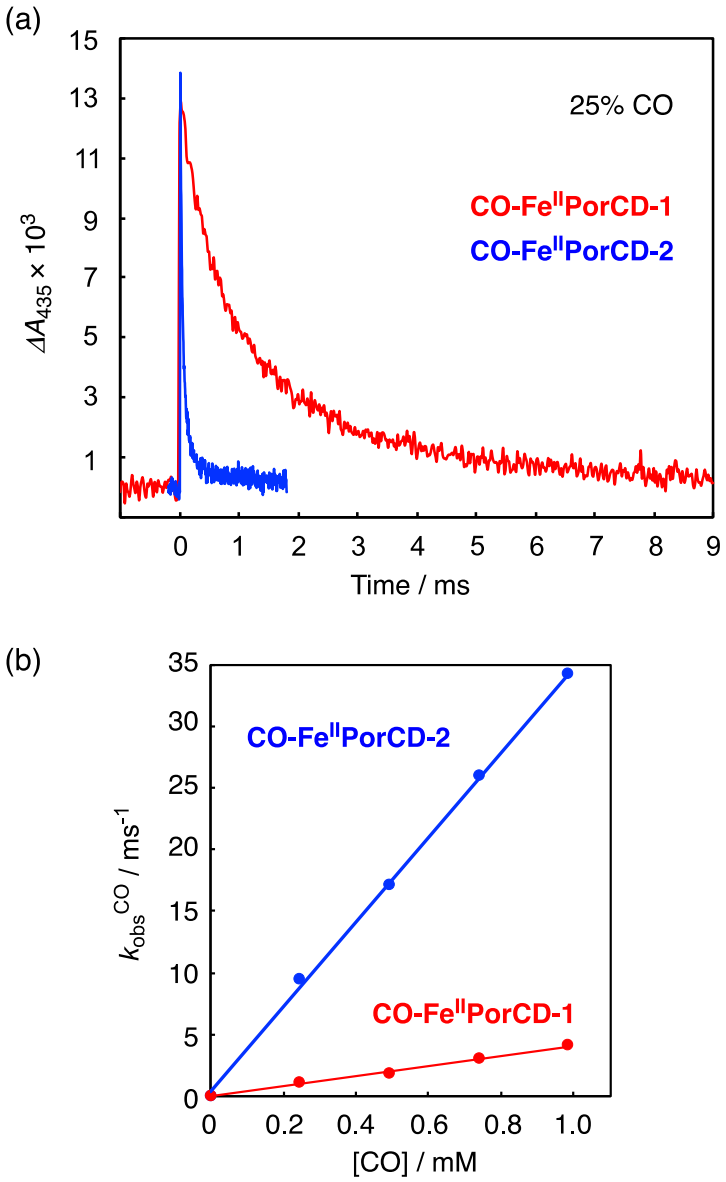

Figure 8. Laser flash photolysis for the kinetic study. (a) The time course for CO association with **Fe^{II}PorCD-1** (red) and **Fe^{II}PorCD-2** (blue) generated by laser flash irradiation (532 nm) to **CO-Fe^{II}PorCD-1** and **CO-Fe^{II}PorCD-2**, respectively, in 0.05 M phosphate buffer at pH 7.0 and 25°C. (b) Plots for the observed rate constants, k_{obs}^{CO}, for CO association with **Fe^{II}PorCD-1** (red) and **Fe^{II}PorCD-2** (blue) versus [CO]. The second order rate constants (k_{on}^{CO}) were determined from the slopes of the linear regression lines.

Table 2. Kinetic parameters for O_2 and CO binding of native Mb and related model compounds at 25°C.

	k_{on}^{CO} (M^{-1} s^{-1})	k_{off}^{CO} (s^{-1})	k_{on}^{O2} (M^{-1} s^{-1})	k_{off}^{O2} (s^{-1})
Mb [a]	(3–5) × 10^5	(1.5–40) × 10^{-3}	(1–2) × 10^7	10–30
Hb-R state [a]	4.6 × 10^6	9 × 10^{-3}	3.3 × 10^7	13.1
Picket-fence Por (DiMeIm) [a]	1.4 × 10^6	0.14	1.1 × 10^8	4600
FePocPiv (1-MeIm) [a]	5.8 × 10^5	8.6 × 10^{-3}	2.2 × 10^6	9
TCP-IM [b]	2.1 × 10^7	0.23	4.0 × 10^7	2.0 × 10^3
TCP-PY [b]	1.6 × 10^7	3.2	2.7 × 10^7	2.5 × 10^3
αα-OCAPFe [c]			9.0 × 10^6	< 1× 10^3
αβ-OCAPFe [c]			> 1.0 × 10^8	> 1.3
hemoCD3 [d]	2.6 × 10^7	0.018	2.0 × 10^8	5.3 × 10^3
Fe^{II}PorCD-1 [d]	4.2 × 10^6	0.11	1.1 × 10^7	115
Fe^{II}PorCD-2 [d]	3.4 × 10^7	0.016	9.8 × 10^7	1.3 × 10^3

[a] Ref (4), [b] Ref (7), [c] Ref (25), [d] This work

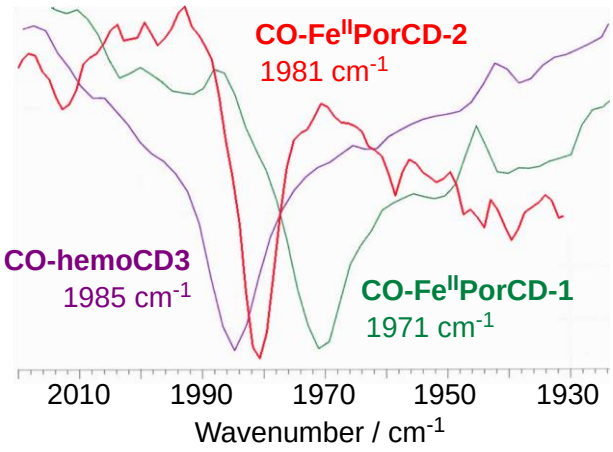

Figure 9. IR spectra of the CO complexes of **hemoCD3**, **Fe^{II}PorCD-1**, and **Fe^{II}PorCD-2** in 0.05 M phosphate buffer at pH 7 and room temperature.

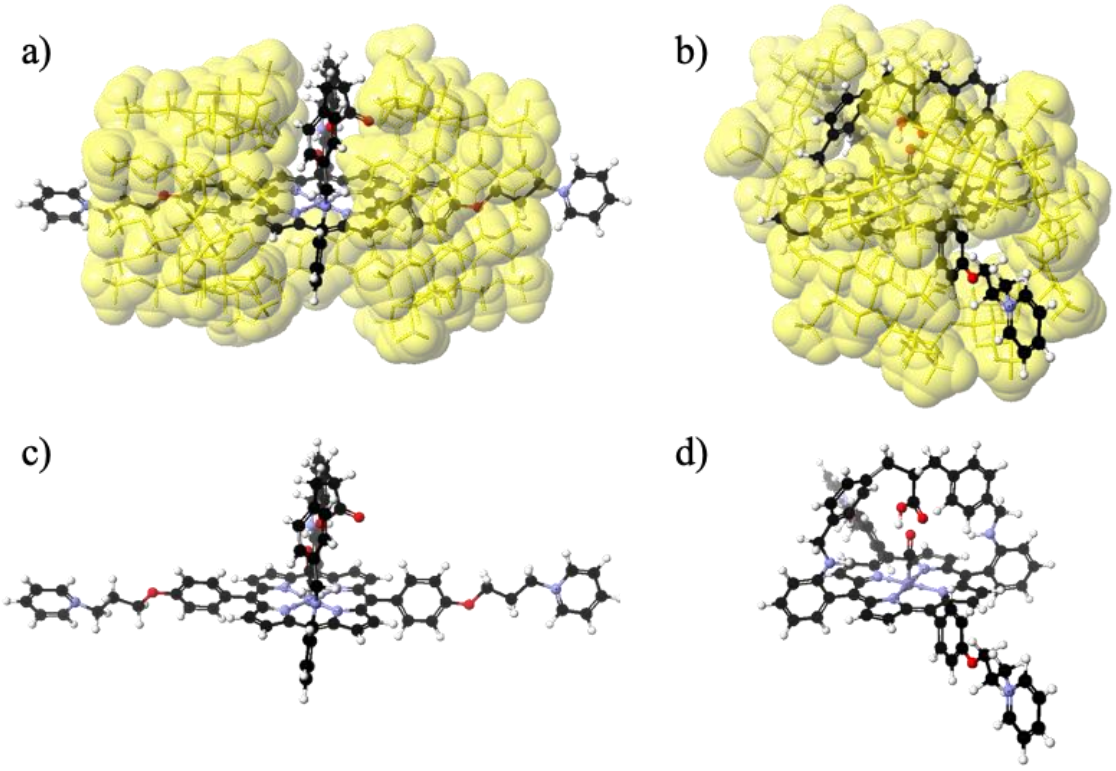

Figure 10. Optimized structures of **CO-Fe^{II}PorCD-1** complex with different angles. The CD dimer, **Py3OCD**, is shown as a yellow half-skeleton in (a) and (b). The yellow half-skeleton is omitted to clearly show the strap structure in (c) and (d). The porphyrins in (a)/(c) and (b)/(d) are set in the same positions and angles. The molecular model was constructed using CONFLEX/MM3 parameters in Scigress version 2.2.1 software program (Fujitsu).

Graphic for Table of Contents (TOC)

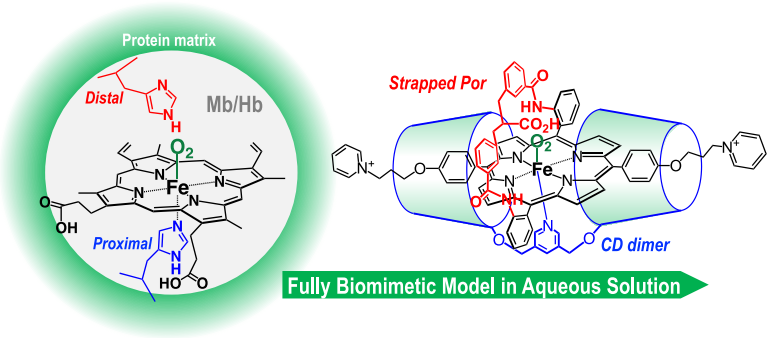

Synopsis: In native hemoglobin (Hb) and myoglobin (Mb), binding to gaseous ligands is regulated by proximal and distal amino acid residues of the heme pocket. To construct a water-soluble Hb/Mb biomimetic model, we report here the supramolecular system composed of a strapped porphyrin bearing overhanging COOH and a methylated β-cyclodextrin dimer with a pyridine ligand. The supramolecular complex showed marked O_2/CO selectivity comparable to native Hb/Mb in aqueous solution.